The Journal of Chemical Physics

Ultrafast laser induced charge migration with de- and re-coherences in polyatomic molecules: A general method with application to pyrene

Cite as: J. Chem. Phys. **158**, 124306 (2023); https://doi.org/10.1063/5.0141631
Submitted: 07 January 2023 • Accepted: 06 March 2023 • Accepted Manuscript Online: 06 March 2023 • Published Online: 24 March 2023

HuiMin Ma, Jörn Manz, HuiHui Wang, et al.

AIP Publishing

The Journal of Chemical Physics ARTICLE scitation.org/journal/jcp

Ultrafast laser induced charge migration with de- and re-coherences in polyatomic molecules: A general method with application to pyrene

Cite as: J. Chem. Phys. 158, 124306 (2023); doi: 10.1063/5.0141631
Submitted: 7 January 2023 • Accepted: 6 March 2023 •
Published Online: 24 March 2023

HuiMin Ma,[1] Jörn Manz,[1,2] HuiHui Wang,[1,a)] YiJing Yan,[3] and Yonggang Yang[1,4,a)]

AFFILIATIONS

[1] State Key Laboratory of Quantum Optics and Quantum Optics Devices, Institute of Laser Spectroscopy, Shanxi University, Taiyuan 030006, China
[2] Institut für Chemie und Biochemie, Freie Universität Berlin, 14195 Berlin, Germany
[3] Department of Chemical Physics, University of Science and Technology of China, Hefei, Anhui 230026, China
[4] Collaborative Innovation Center of Extreme Optics, Shanxi University, Taiyuan 030006, China

[a)] **Author to whom correspondence should be addressed:** huihuiwang2019@sxu.edu.cn and ygyang@sxu.edu.cn

ABSTRACT

We develop a general method to study ultrafast laser induced charge migration in molecules, which includes both electronic and nuclear dynamics. The method can be applied to relatively large systems. A detailed analysis of charge migration in pyrene is performed. Decoherences and recoherences of charge migration in pyrene are found and explained in terms of nuclear motions.

I. INTRODUCTION

Charge migration is the process by which electrons or electron holes are moved in molecules or molecular ions over one to several bond distances on a time scale ranging from several hundred attoseconds to a few femtoseconds. There are many variants. For example, the charge may run from one end to the opposite end of a linear or quasi-linear molecule,[1–13] or it may circulate in a planar molecule or around a linear molecule,[7,14–20] or it may run along a helical path around a linear molecule.[21] For surveys, perspectives, and supplementary guidance to the literature, see Refs. 10, 13, 22, and 23. Moreover, there are stimulating analogies between electronic charge migration and nuclear tunneling.[24]

The simplest quantum mechanical representation of the process is in terms of a coherent superposition of two electronic eigenfunctions, typically for the electronic ground state and one excited state, for the scenario of fixed nuclei. In this ideal case, the charge migrates periodically forever. This scenario may serve as a reference. It is motivated by the much shorter time scale of electronic motions compared to nuclear motions, due to the much smaller mass of electrons compared to nuclei. More realistic quantum dynamics simulations of charge migration should account, however, for the effects of nuclear motions. In general, these effects may be summarized as in the recent perspective by Shu and Truhlar.[25] Accordingly, electrons and nuclei may be considered as system ("A") and environment ("B"), or as two sub-systems of the composite system AB, i.e., of the molecule. Their interaction causes decoherence in the coherent motion of the system. The effect was discovered first for charge migration in the simplest molecular ion, i.e., in H_2^+ prepared in the superposition of the electronic ground and first excited states. For the reference model of fixed nuclei, the electron ("A") migrates periodically forever.[1,5,26] The coupling to nuclear motions ("B") causes decoherence within several femtoseconds.[27] Subsequently, the phenomenon has been confirmed for charge migrations in many molecules or molecular ions (see, e.g., Refs. 13, 25, and 28–38).

Nuclear motions do not only cause decoherence of charge migration. They may even induce (partial) recoherences. This phenomenon was discovered first by quantum dynamics simulations of charge migration in diatomic molecules.[28,32] Vacher *et al.*[34] pointed to the possibility of the phenomenon also occurring in small polyatomic molecules, but their results for paraxylene[34] could not be

confirmed in Ref. 33. Subsequently, the effect was documented for the linear iodo-acetylenic cation[39] (see also Ref. 40) and in the model fulvene with a reduced set of five different totally symmetric modes (out of 24) in the ground state and one excited electronic state.[41] Today, the predictions culminate in a triumph: charge migration with de- and recoherences has been observed and analyzed in silane (SiH_4), both experimentally and theoretically.[38]

The general model of charge migration with de- and recoherences has stimulated the development of various methods for quantum dynamics simulations; for recent surveys see Refs. 13, 23, and 25. Usually, these methods do not describe the initiation of charge migration by means of a laser pulse. Instead, they assume that initially, at time $t = 0$, the laser pulse has prepared the system (e.g., a molecular ion) in a superposition of electronic states, e.g., the electronic ground ($|g\rangle$) and one or more excited states ($|e\rangle$) (e.g., by sudden photoionization of the neutral precursor; equivalent initial states can also be generated by photoexcitation of the ion from $|g\rangle$ to a superposition of $|g\rangle$ and $|e\rangle$[42]). The subsequent field-free time evolution is then represented by the total molecular wavefunction $\Psi(\mathbf{q}, \mathbf{Q}, t)$ which depends on the electronic and nuclear coordinates $\mathbf{q}$ and $\mathbf{Q}$.

It is common practice to expand the field-free molecular wavefunction $\Psi(\mathbf{q}, \mathbf{Q}, t)$ in terms of products of electronic state-($|a\rangle$)-selective eigenfunctions $\Phi_a(\mathbf{q}; \mathbf{Q})$ times time-dependent normalized nuclear wave functions $\chi_a(\mathbf{Q}; t)$ times amplitudes, which determine the probabilities of occupying states $|a\rangle$ and the phases. This ansatz corresponds to the familiar Born–Huang expansion of the molecular (AB) wavefunction in terms of products of electronic (A) times nuclear (B) wavefunctions[43] (see also Refs. 44–47). As approximation which may be called the adiabatic Born–Huang expansion, each nuclear wavefunction moves independently on its electronic-state-($|a\rangle$)-specific potential energy surface (PES) $V_a(\mathbf{Q})$. This ansatz is equivalent to a set of independent, electronic state-specific Born–Oppenheimer dynamics without any nonadiabatic transitions between the states. This approximation neglects the kinetic couplings; e.g., it cannot account for the effects of conical intersections.

For special applications, the adiabatic Born–Huang expansion may even be restricted to just two electronic states, typically the electronic ground state ($|a\rangle = |g\rangle$) and one excited state ($|a\rangle = |e\rangle$). As an impressive example, this "minimal" adiabatic Born–Huang expansion has been successfully applied to about 250 small-to-medium sized organic molecules for a systematic search for charge migrations with long-lasting electronic coherences.[37] The longest decoherence times discovered this way are of the order of 10 fs. Recently, a new "record" of decoherence time, i.e., ~15 fs, in silane (SiH_4) has been discovered both experimentally and quantum dynamically,[38] followed by recoherence at 40–50 fs. In an alternative model with so-called Ehrenfest dynamics,[48] the nuclear wavefunctions (or representative ensembles of trajectories) move rather slowly on a rather shallow PES, which is constructed as the mean value of a steeper state-selective $V_a(\mathbf{Q})$—this can mislead to artificial decoherence times that exceed the correct results by an order of magnitude (compare, e.g., the results for the decoherence times in $HCCI^+$ in Refs. 10 and 39 with and without Ehrenfest dynamics).

In this context, the present work has two purposes: method development and the search for criteria that support charge migration with de- and recoherences in rather large polyatomic molecules. The criteria will be derived from the results of the application to pyrene, a touchstone larger than all other candidates that have been investigated previously. This makes the application exceedingly challenging because "the loss of coherence"—and we may add, the suppression of recoherences—"can be expected to occur even faster if more (vibrational) modes are included" (quoted from Ref. 33).

Concerning the methods, we adapt the adiabatic Born–Huang expansion of the total wavefunction in full dimensionality, which means with all vibrational modes, with three extensions: First, to describe the initiation of the charge migration by an ultrashort laser pulse. Second, to present the resulting time-dependent electron density in real space such that it illustrates the charge migration with de- and recoherences directly. In contrast, most of the previous investigations present the phenomenon in a way that we consider indirect, namely, in terms of the (overlap of) nuclear wavefunctions (see, e.g., Refs. 13, 31, 33, 36, and 37). Third, to document the phenomenon in terms of the corresponding electronic flux. It is well known that fluxes allow illuminating visualizations of the dynamics, e.g., with prominent time-dependent switches of the flux directions even when the resulting changes in the density are hardly visible.[24,49] The bulk of the methods are presented in Sec. II, with a small addition for the electronic flux in Sec. III. The derivations are for arbitrary sets of electronic states and for all vibrational modes of the polyatomic molecule, which means in full dimensionality. Section II also specifies additional approximations. The application in Sec. III employs the minimal adiabatic Born–Huang expansion.

For the application, we choose the model pyrene with 72 vibrational modes. Its planar structure with D_{2h} symmetry in the electronic ground state is shown in Fig. 1. Four of the vibrational modes are also illustrated in Fig. 1.

Our choice of pyrene for the application of the general theory has two motivations: First, the superposition of the electronic ground state (A_g) and the first bright state (B_{1u}, also labeled ^1L_a according to Ref. 50) has been realized experimentally to study the time-dependent population of the excited state.[51,52] Coherence is created by two time-delayed laser pulses. The observations point to decoherence and partial recoherence. As a working hypothesis, this suggests charge migration with de- and recoherences in pyrene, the largest polyatomic molecule that has been investigated so far.

Second, there are successful quantum chemical and quantum dynamical studies of various complementary properties of pyrene.[53,54] These provide robust theoretical bases for the present extended investigation of the charge migration in pyrene. In particular, the experimentally resolved vibrational absorption spectrum in the ultraviolet–visible (UV–vis) range[55–57] is well reproduced by calculations in the frame of the minimal adiabatic Born–Huang expansion for the electronic ground state and the first bright state with all (72) vibrational modes.[53] Here we adapt the model and some of the quantum chemical methods that have been employed in Ref. 53. Details are in Sec. II.

We admit from the outset, however, that the model adapted from Ref. 53 neglects the coupling between the bright B_{1u} state and the dark B_{2u} state (also labeled ^1L_b[50]) of pyrene. According to semi-classical on-the-fly dynamical calculations of Ref. 54, this induces population transfer after the preparation of the $A_g + B_{1u}$ superposition. This causes depopulation of the bright state with a time constant of 43 fs, in reasonable agreement with the experimental value of 85 fs.[52] Therefore, as a conservative estimate, the

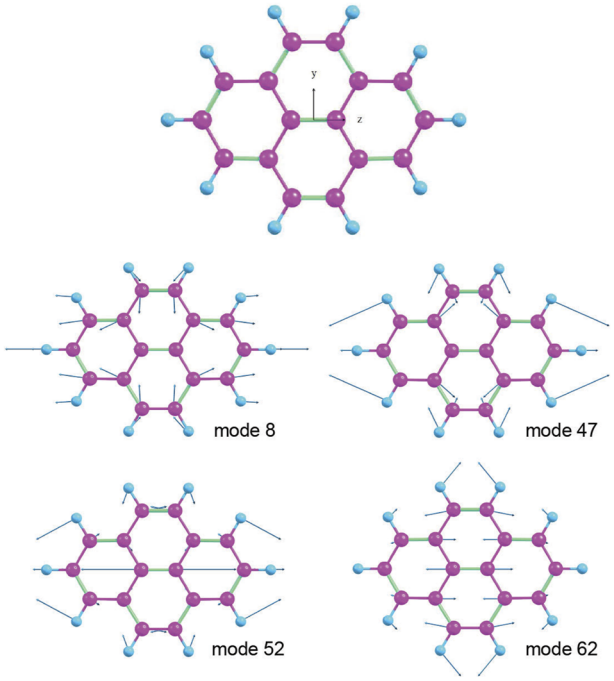

FIG. 1. Optimized planar equilibrium structure of pyrene in the electronic ground state $|g\rangle = |A_g\rangle$, adapted from Ref. 53. The symmetry is D_{2h}. The molecule is placed in the yz plane, with its center of mass at the origin. For the scaling, the length of the arrows along y and z is 1 Å. The arrow plots illustrate four vibrational modes labeled $j = 8$, 47, 52, and 62.

present quantum dynamical results can predict the properties of charge migration just for a rather short time (<43 fs). They cannot account quantitatively for the subsequent spectral signatures of the recoherence, which are rather weak.[51,52] Gratifyingly, however, any population of the dark state B_{2u} would not contribute to charge migration along the z-axis, which will be investigated in this work, due to symmetry reasons. Therefore, even though the present model is not perfect, we are nevertheless confident that it should account for the essential properties of laser induced charge migration. The corresponding results for the model system pyrene should allow for the discovery of some rather general criteria for observing charge migration with de- and recoherences in rather large molecules. Moreover, it should also explain an intriguing new effect that has been observed experimentally, i.e., the phase shift of recoherence.[51,52]

The theory, model, and methods are presented in Sec. II in a comprehensive and self-consistent manner. The results and discussions are in Sec. III, using the terminology that was introduced in Sec. II. The conclusions are in Sec. IV.

II. METHODS

A. Electronic and nuclear dynamics under external field

As our first extension of the familiar description of field-free charge migration with de- and recoherences by means of the adiabatic Born–Huang expansion (cf. Sec. I), here we develop a method for quantum dynamics simulation of the initiation of the process by means of an ultrafast (~1 fs) laser pulse.

Beside the initial electronic ground state $|a = g\rangle$, the ultrafast laser field, $\varepsilon(t)$, engages coherently some quasi-bound excited electronic states $|a = e\rangle$. Let $\mathbf{Q}$, $\mathbf{Q}_a^{eq}$, and $\mathbf{P}$ be the collective nuclear coordinate, the equilibrium coordinate in state $|a\rangle$, and the momentum, respectively. In a semiclassical approximation of the coupling of the molecular dipole (μ) to the laser field $\varepsilon(t)$, the molecular vibronic Hamiltonian in the presence of the external laser field reads

$$\hat{H}(t) = \sum_{ab} \{\delta_{ab}[H_a(\mathbf{Q},\mathbf{P}) + E_a] - \varepsilon(t)\mu_{ab}(\mathbf{Q})\}|a\rangle\langle b|. \quad (1)$$

For convenience, the corresponding potential energy surface (PES) of state $|a\rangle$ is separated into two parts, $E_a + V_a(\mathbf{Q})$, where E_a is the minimum value at $\mathbf{Q}_a^{eq}$, and $V_a(\mathbf{Q})$ denotes the $\mathbf{Q}$-dependent part, with $V_a(\mathbf{Q}_a^{eq}) = 0$. We set $E_g = 0$ and $\mathbf{Q}_g^{eq} = \mathbf{0}$. The nuclear Hamiltonian $H_a(\mathbf{Q},\mathbf{P})$ accounts for $V_a(\mathbf{Q})$ and for the nuclear kinetic energy in state $|a\rangle$. The corresponding electronic wave function is $\langle \mathbf{q}|a\rangle = \Phi_a(\mathbf{q};\mathbf{Q})$ with $\mathbf{q}$ being the collective electronic coordinate.

The total wave function, $\langle \mathbf{q}|\Psi(\mathbf{Q},t)\rangle$, satisfies

$$i\hbar\frac{\partial}{\partial t}|\Psi(\mathbf{Q},t)\rangle = \hat{H}(t)|\Psi(\mathbf{Q},t)\rangle. \quad (2)$$

Our (approximate) solution of this time-dependent Schrödinger equation starts from the Born–Huang-type expansion (cf. Sec. I),

$$|\Psi(\mathbf{Q},t)\rangle = \mathcal{N}^{-\frac{1}{2}}\sum_a e^{-iE_at/\hbar}\Psi_a(\mathbf{Q},t)|a\rangle, \quad (3)$$

with normalization

$$\mathcal{N} = \sum_a \int d\mathbf{Q}\,|\Psi_a(\mathbf{Q},t)|^2. \quad (4)$$

Here the electronic-state-($|a\rangle$)-specific nuclear wavefunctions satisfy

$$i\hbar\frac{\partial}{\partial t}\Psi_a(\mathbf{Q},t) = \sum_b [\delta_{ab}H_a(\mathbf{Q},\mathbf{P}) - \varepsilon(t)\mu_{ab}(\mathbf{Q},t)]\Psi_b(\mathbf{Q},t), \quad (5)$$

where $\mu_{ab}(\mathbf{Q},t) = \mu_{ab}(\mathbf{Q})e^{i\omega_{ab}t}$ with $\omega_{ab} = \frac{E_a - E_b}{\hbar}$.

The coupled set of Eq. (5) means that the nonadiabatic couplings are neglected and the electronic transitions are mediated exclusively by the laser-dipole couplings. Accordingly, in the absence of the external field, Eq. (5) describes the adiabatic nuclear dynamics without surface crossing. This is the adiabatic approximation to the Born–Huang-type expansion. To that end, we set

$$\Psi_a(\mathbf{Q},t) \equiv \psi_a(t;\mathbf{Q})\chi_a(\mathbf{Q},t), \quad (6)$$

for the vibronic wave function. As usual, the normalized nuclear wavepacket $\chi_a(\mathbf{Q},t)$ obeys the electronic-state-($|a\rangle$)-specific adiabatic Born–Oppenheimer dynamics,

$$i\hbar\frac{\partial}{\partial t}\chi_a(\mathbf{Q},t) = H_a(\mathbf{Q},\mathbf{P})\chi_a(\mathbf{Q},t). \quad (7)$$

However, the ansatz (6) multiplies $\chi_a(\mathbf{Q},t)$ by the factor $\psi_a(t;\mathbf{Q})$, to account for electronic transitions induced by the laser. It is to be determined first at the fixed nuclear configuration $\mathbf{Q}$, under the influence of the external field. The field-free adiabatic nuclear dynamics of $\Psi_a(\mathbf{Q},t)$, with its propagated electronic component at the end of the ultrafast laser pulse, will then follow (cf. Sec. II B).

More specifically, during the laser pulse, the nuclear wave function component is described by

$$i\hbar\chi_a(\mathbf{Q},t)\frac{\partial}{\partial t}\psi_a(t;\mathbf{Q}) = -\varepsilon(t)\sum_b \mu_{ab}(\mathbf{Q},t)\psi_b(t;\mathbf{Q})\chi_b(\mathbf{Q},t). \quad (8)$$

We need the solution to this equation only for the ultrashort duration of the laser pulse. For such a short duration, it is reasonable to assume $\chi_a(\mathbf{Q},t) \approx \chi_b(\mathbf{Q},t)$. Equation (8) is thus reduced to

$$i\hbar\frac{\partial}{\partial t}\psi_a(t;\mathbf{Q}) = -\varepsilon(t)\sum_b \mu_{ab}(\mathbf{Q},t)\psi_b(t;\mathbf{Q}). \quad (9)$$

Due to the fast oscillations of the laser field, the contributions $-\varepsilon(t)\mu_{aa}(\mathbf{Q})$ of the permanent dipole moments are averaged to zero. Consequently, we neglect these terms. The parametrical dependence of $\psi_a(t;\mathbf{Q})$ on $\mathbf{Q}$ arises from the non-Condon property of the transition dipole. The normalization is

$$\sum_a |\psi_a(t;\mathbf{Q})|^2 = 1. \quad (10)$$

This holds for an individual $\mathbf{Q}$ that is treated as a parameter. In the Condon approximation, we would obtain $\psi_a(t;\mathbf{Q}) \to c_a(t)$, with the dependence on the nuclear configuration being concerted.

Now consider the preparation of the molecule by an ultrashort laser field,

$$\varepsilon(t) \neq 0, \quad \text{only when} \quad t \in (t_0, 0). \quad (11)$$

The system was initially in the electronic ground state $|g\rangle$, prior to the action of $\varepsilon(t)$. Therefore,

$$\psi_a(t_0;\mathbf{Q}) = \delta_{ag}. \quad (12)$$

For $\varepsilon(t>0)=0$, Eq. (9) results in

$$\psi_a(t>0;\mathbf{Q}) = \psi_a(t=0;\mathbf{Q}). \quad (13)$$

B. Adiabatic nuclear dynamics and initial values

After the laser pulse, the wavefunction that has been determined in Sec. II A evolves according to the familiar adiabatic Born–Huang-type approach (cf. Sec. I). Apparently, for $t>0$, Eq. (6) is simplified by Eq. (13),

$$\Psi_a(\mathbf{Q};t) \equiv \psi_a(0;\mathbf{Q})\chi_a(\mathbf{Q};t). \quad (14)$$

Moreover, since $\varepsilon(t>0)=0$, as specified in Eq. (11), the field-free Eq. (5) reduces to

$$i\hbar\frac{\partial}{\partial t}\Psi_a(\mathbf{Q},t) = H_a(\mathbf{Q},\hat{\mathbf{P}})\Psi_a(\mathbf{Q},t). \quad (15)$$

That means the nuclear wavefunctions evolve adiabatically. In principle, the initial value for Eq. (14) should be determined with the coupled electron and nuclear dynamics via Eq. (5) in the presence of an excitation field. This is numerically feasible for small molecules. Adopted below is a simplified and intuitive method for the scenario of ultrafast laser excitation. Let $\chi_{g,\mathbf{n}}(\mathbf{Q})$ be the initial normalized nuclear wave function, satisfying $H_g(\mathbf{Q},\mathbf{p})\chi_{g,\mathbf{n}}(\mathbf{Q}) = E_{g,\mathbf{n}}\chi_{g,\mathbf{n}}(\mathbf{Q})$. Here, the boldface vibration index, $\mathbf{n}$, specifies the vibrational quantum numbers of the multiple-modes of a polyatomic molecule. The corresponding initial value of Eq. (14), upon an ultrafast laser excitation, then simplifies to

$$\Psi_a(\mathbf{Q},t=0) = \psi_a(0;\mathbf{Q})\chi_{g,\mathbf{n}}(\mathbf{Q}). \quad (16)$$

For an explicit example, see Ref. 39.

It is worth noting that $\psi_a(0;\mathbf{Q})$ has been completely determined, satisfying Eqs. (9)–(13). While Eq. (15) is norm-conserving, $\Psi_a(\mathbf{Q},t)$ via Eq. (16) is not individually normalized. It is the total vibronic wave function, $|\Psi(\mathbf{Q},t)\rangle$ of Eq. (3), which is normalized over the entire electron–and–nuclear space. The normalization constant, $\mathcal{N}$ of Eq. (4), which is time-independent, is now completely determined for any given initial value of Eq. (16).

C. Gaussian wavepacket dynamics

For the present purpose, i.e., quantum dynamics simulations of charge migration with de- and recoherences in polyatomic molecules, the calculation of the adiabatic high-dimensional time evolution of the nuclear wavefunctions as the solution of the nuclear Schrödinger equation Eq. (15) with an initial value of (14) is still a formidable task. Here we adapt an approximation that yields a rather simple solution and that has been successfully applied to many polyatomic molecules, namely, in terms of products of time-dependent Gaussians, originally proposed by Heller[58] (cf. Refs. 13, 36, 37, 59, and 60).

The derivation and implementation start from the Condon approximation, assuming the electronic transition dipoles to be constants, i.e.,

$$\mu_{ab}(\mathbf{Q}) \approx \mu_{ab} \equiv \mu_{ab}(\mathbf{Q}_g^{eq}). \quad (17)$$

They are evaluated at the minimum of the potential energy surface of the ground state. The resultant $\{\psi_a(0;\mathbf{Q})\}$ via Eqs. (9)–(13) are constants and read

$$\psi_a(t=0;\mathbf{Q}) \equiv c_a. \quad (18)$$

The rest of the derivation follows Refs. 13, 36, 37, and 58–60. It is reproduced here in order to introduce the notations that are used subsequently for the presentations of the results. Accordingly, each electronic-state-($|a\rangle$)-specific nuclear Hamiltonian represents a collection of N harmonic oscillators, i.e.,

$$H_a(\mathbf{Q},\mathbf{P}) = \sum_{j=1}^{N}\left[\frac{P_j^2}{2} + \frac{1}{2}\omega_{aj}^2(Q_j - Q_{aj}^{eq})^2\right]. \quad (19)$$

Here, Q_j and P_j denote the mass-weighted coordinate and momentum of the jth–normal mode. There are no Dushinsky rotations. The locations $Q_{aj}^{eq} = \hat{\mathbf{e}}_j \cdot \mathbf{Q}_a^{eq}$ of the potential minima and the frequencies ω_{aj} depend on the electronic-state a and the mode j, where $\hat{\mathbf{e}}_j$ is the

normal-mode unit vector of mode j. For $t > 0$, the N-mode adiabatic wave function in Eq. (14) can then be factorized as

$$\chi_a(\mathbf{Q}, t) = \prod_{j=1}^{N} \chi_{aj}(Q_j, t). \tag{20}$$

The initial harmonic system is in the ground state $\chi_{g,\mathbf{n}}(\mathbf{Q}) = \chi_{g,\mathbf{0}}(\mathbf{Q})$. The initial wavepacket is thus

$$\chi_{aj}(Q_j, t = 0) = N_j e^{-\alpha_{gj} Q_j^2}, \tag{21}$$

where

$$N_j \equiv \left(\frac{2\alpha_{gj}}{\pi}\right)^{\frac{1}{4}}, \quad \text{and} \quad \alpha_{aj} \equiv \frac{\omega_{aj}}{2\hbar}. \tag{22}$$

Each $\chi_{aj}(Q_j, t)$ is governed by the individual normal-mode Hamiltonian in Eq. (19), with the potential,

$$V_a(Q_j) = \frac{1}{2}\omega_{aj}^2 (Q_j - Q_{aj}^{eq})^2. \tag{23}$$

As a consequence, $\chi_{aj}(Q_j, t)$ keeps the form of a Gaussian wavepacket (GWP).[60] The norm of the initial wave function has already been specified in Eqs. (21) and (22). The generic form of GWP is then written as[58–60]

$$\chi_{aj}(Q_j, t) = N_j \exp\left[-\alpha_{ajt}(Q_j - Q_{ajt})^2 + \frac{i}{\hbar} P_{ajt}(Q_j - Q_{ajt}) + \frac{i}{\hbar}\gamma_{ajt}\right]. \tag{24}$$

One can then readily express the wave function dynamics in terms of the time-dependent GWP parameters, $\{\alpha_{ajt}, Q_{ajt}, P_{ajt}, \gamma_{ajt}\}$.

The standard GWP dynamics method leads to[59]

$$\begin{aligned} Q_{ajt} &= Q_{aj}^{eq}[1 - \cos(\omega_{aj} t)], \\ P_{ajt} &= \omega_{aj} Q_{aj}^{eq} \sin(\omega_{aj} t), \\ \alpha_{ajt} &= \alpha_{aj}\left[\frac{\alpha_{gj}\cos(\omega_{aj} t) + i\alpha_{aj}\sin(\omega_{aj} t)}{\alpha_{aj}\cos(\omega_{aj} t) + i\alpha_{gj}\sin(\omega_{aj} t)}\right], \\ \gamma_{ajt} &= \frac{1}{2}P_{ajt}Q_{ajt} + \frac{i\hbar}{2}\ln\left(\frac{i\omega_{gj}\sin(\omega_{aj} t) + \omega_{aj}\cos(\omega_{aj} t)}{\omega_{aj}}\right). \end{aligned} \tag{25}$$

D. The time-dependent electron density in real space

We now turn to the second extension of the established theory for charge migration with de- and recoherences, aiming at a direct representation of the phenomenon in terms of the electron density in real space. In contrast, most previous representations describe the electronic decoherence in terms of the (overlaps of) nuclear wavefunctions (cf. Refs. 13, 31, 34, and 36–38). For our purpose, it is helpful to remind ourselves of the general view presented by Shu and Truhlar,[25] which considers the molecule as a composite system ("AB") of the system ("A," the electrons) and the environment ("B," the nuclei). The reduced density of the system ("A") is then obtained by integrating the total molecular ("AB") density over the degrees of freedom of the environment ("B").

Accordingly, the derivation starts from the total wave function is $\Psi(\mathbf{q}, \mathbf{Q}, \mathbf{R}_g, t)$, where $\mathbf{R}_g$ represents the global translational and rotational DOFs. The speed of $\mathbf{R}_g$ is several orders of magnitude smaller compared to the speed of charge migration. We mainly focus on charge migration for $t > 0$, therefore, we neglect the slow contributions due to motions of $\mathbf{R}_g$. The relevant total wavefunction of the composite system ("AB") is thus $\Psi(\mathbf{q}, \mathbf{Q}, t)$ after $\mathbf{R}_g$ is separated. It takes the familiar form of the adiabatic Born–Huang-type expansion,

$$\Psi(\mathbf{q}, \mathbf{Q}, t) = \sum_a c_a e^{-iE_a t/\hbar} \Phi_a(\mathbf{q}; \mathbf{Q}) \chi_a(\mathbf{Q}, t). \tag{26}$$

Accordingly, the reduced density of the system ("A," the N electrons) can be obtained by integration of the total density $\Psi^*(\mathbf{q}, \mathbf{Q}, t)\Psi(\mathbf{q}, \mathbf{Q}, t)$ over $\mathbf{Q}$. Then the electron density in real space can be obtained by further integration over $N - 1$ of the N electrons,

$$\rho_{el}(\mathbf{r}, t) = \sum_{a,b} c_a^* c_b e^{-i(E_b - E_a)t/\hbar} \int d\mathbf{Q} \rho_{ab}(\mathbf{r}, \mathbf{Q}) \chi_a^*(\mathbf{Q}, t) \chi_b(\mathbf{Q}, t), \tag{27}$$

where $\rho_{ab}(\mathbf{r}, \mathbf{Q}) = \int d\mathbf{q} \Phi_a^*(\mathbf{q}; \mathbf{Q}) \sum_i \delta(\mathbf{r} - \mathbf{r}_i) \Phi_b(\mathbf{q}; \mathbf{Q})$. Here, $\mathbf{r}_i$ is the spatial coordinate of the ith electron. Since the core electrons just follow the motions of the nuclei and do not contribute to charge migration, in the following we only consider the valence electrons. We use the same notations ρ_{el}, Φ_a, ρ_{ab}, but now they are only the part for valence electrons.

To evaluate the electron density Eq. (27), we use the Taylor expansion

$$\begin{aligned} \rho_{ab}(\mathbf{r}, \mathbf{Q}) = \rho_{ab}^{(0)}(\mathbf{r}) &+ \sum_j \rho_{ab,j}^{(1)}(\mathbf{r})(Q_j - Q_j^{ab}) \\ &+ \frac{1}{2}\sum_{j_1 j_2} \rho_{ab,j_1 j_2}^{(2)}(\mathbf{r})(Q_{j_1} - Q_{j_1}^{ab})(Q_{j_2} - Q_{j_2}^{ab}) + \cdots. \end{aligned} \tag{28}$$

For short notations, define

$$\begin{aligned} C_{ab}(t) &= c_a^* c_b e^{-i(E_b - E_a)t/\hbar}, \\ S_{ab}(t) &= \int d\mathbf{Q} \chi_a^*(\mathbf{Q}, t) \chi_b(\mathbf{Q}, t) \equiv \prod_{j=1}^{N} S_{ab,j}(t), \\ \langle Q_j^n(t)\rangle_{ab} &= \int dQ_j \chi_{aj}^*(Q_j, t)(Q_j - Q_j^{ab})^n \chi_{bj}(Q_j, t), \quad n = 0, 1, \ldots \\ S_{ab,j}(t) &= \int \chi_{aj}^*(Q_j, t)\chi_{bj}(Q_j, t) dQ_j = \langle Q_j^0(t)\rangle_{ab}. \end{aligned} \tag{29}$$

Insertion of Eq. (28) into Eq. (27) calls for integration of the zeroth, first, second, etc. order terms of Eq. (28) over the nuclear coordinates $\mathbf{Q}$. For example, using the definitions in Eq. (29), we obtain the first order term $\int dQ(Q_j - Q_j^{ab})\chi_a^*(\mathbf{Q}, t)\chi_b(\mathbf{Q}, t) = \frac{S_{ab}(t)\langle Q_j(t)\rangle_{ab}}{S_{ab,j}(t)} = \frac{S_{ab}(t)\langle Q_j(t)\rangle_{ab}}{\langle Q_j^0(t)\rangle}$. The electron density is thus evaluated as

$$\begin{aligned} \rho_{el}(\mathbf{r}, t) = \sum_{ab} C_{ab}(t) S_{ab}(t) \Bigg\{ &\rho_{ab}^{(0)}(\mathbf{r}) + \sum_j \rho_{ab,j}^{(1)}(\mathbf{r}) \frac{\langle Q_j(t)\rangle_{ab}}{\langle Q_j^0(t)\rangle_{ab}} \\ &+ \frac{1}{2}\sum_{j_1 j_2} \rho_{ab,j_1 j_2}^{(2)}(\mathbf{r}) \frac{\langle Q_{j_1}(t) Q_{j_2}(t)\rangle_{ab}}{\langle Q_{j_1}^0(t) Q_{j_2}^0(t)\rangle_{ab}} + \cdots \Bigg\}. \end{aligned} \tag{30}$$

If we truncate the expansion Eq. (28) up to first order (linear term), it leads to the so called double harmonic approximation,[61] which is widely used in various quantum chemistry softwares. In this case,

$$\rho_{\rm el}(\mathbf{r},t) = \sum_{ab} C_{ab}(t) S_{ab}(t) \left\{ \rho_{ab}^{(0)}(\mathbf{r}) + \sum_j \rho_{ab,j}^{(1)}(\mathbf{r}) \frac{\langle Q_j(t)\rangle_{ab}}{S_{ab,j}(t)} \right\}. \quad (31)$$

It is remarkable that the factors $C_{ab}(t)$ and $S_{ab}(t)$ depend on the amplitudes and on the overlap of the nuclear wavefunctions in the adiabatic Born–Huang expansion. These quantities have been used to document and quantify the decoherence of charge migration in most previous publications.[13,31,34,36–38] In our derivation, they appear as factors that multiply the nuclear-motion-dependent density matrix elements. This extension allows our direct (graphical) representation of charge migration in terms of the electron density.

The integrations $S_{ab}(t)$ can be obtained analytically for harmonic oscillators. The parameters $\rho_{ab}^{(0)}(\mathbf{r})$, $\rho_{ab,j}^{(1)}(\mathbf{r})$, $\rho_{ab,j_1j_2}^{(2)}(\mathbf{r})$, ..., can be obtained from quantum chemistry calculations at the corresponding fixed geometries $\mathbf{Q}^{ab}$ (see the application in Sec. III A). For simplicity, we set all $\mathbf{Q}^{ab} = \mathbf{Q}_g^{eq}$. For the subsequent application in Sec. III, we adapt the "minimal" version of the adiabatic Born–Huang expansion, which means we only consider two electronic states, the ground state $|a = g\rangle$ and an excited state $|a = e\rangle$. In passing, we shall also present the third extension of the methods, namely, from the presentation of the charge migration by electron densities to fluxes.

III. APPLICATION TO CHARGE MIGRATION IN PYRENE

A. Molecular properties and initial condition

Applications of the theory presented in Sec. II, specifically the "minimal" adiabatic Born–Huang expansion method for the evaluation of charge migration in polyatomic molecules require the calculation of various molecular properties as input. Here, for the model pyrene with the electronic ground state $|g\rangle = |A_g\rangle$ and the first bright excited state $|e\rangle = |B_{1u}\rangle$, it is convenient to adapt several results from Ref. 53. Particularly, Ref. 53 provides the planar D_{2h} equilibrium structure in the ground state $|g\rangle$, as shown in Fig. 1, together with the vibrational frequencies ω_{gj} and ω_{ej} for states $|g\rangle$ and $|e\rangle$. Moreover, detailed analyses in Ref. 53 reveal that Dushinsky rotations in pyrene are negligible. These results were calculated in Ref. 53 by means of the DFT/TDDFT method at the PBE0/def2-TZVP level of theory. We adapt the same method and level of theory from Ref. 53 to calculate some of the required complementary properties of pyrene, which are not available in Ref. 53. For this purpose, we employ the Gaussian 09 suite of programs.[62] In particular, this yields the planar D_{2h} equilibrium structure in the excited state $|e\rangle$. It turns out that the difference between the two equilibrium structures in states $|e\rangle$ and $|g\rangle$ is very small—in fact, it is below the graphical resolution of Fig. 1. This result is in accord with Ref. 54. Gratifyingly, this ensures the validity of the approximations used in Sec. II.

The calculated value of the vertical excitation energy from the ground state $|g\rangle$ to the first bright excited state $|e\rangle$, $\Delta E_{eg}^{\rm vertical}$ = 3.78 eV is also adapted from Ref. 53. It agrees well with the reported experimental value, $\Delta E_{eg,\rm exp}^{\rm vertical}$ = 3.82 eV.[56,57] For comparison, we calculate the energy E_e = 3.63 eV of the equilibrium structure of the excited state. The energy difference $\Delta E_{eg}^{\rm vertical} - E_e$ = 0.15 eV can be well approximated as $\frac{1}{2}\sum_j \omega_{ej}^2 (Q_{ej}^{eq} - Q_{gj}^{eq})^2 = \frac{1}{2}\sum_j \omega_{ej}^2 Q_{ej}^{eq2}$. This supports the applicability of the harmonic approximation for the example of the model pyrene.

In addition, we calculate the value 1.71 ea_0 of the transition dipole moment along the z-axis at the same level of theory. A more accurate value of the transition dipole can be obtained by many-electron wavefunctions calculated at post-HF levels. Therefore, we performed state-averaged CASSCF(12,18) calculations with the same def2-TZVP basis set using MOLPRO.[63] The transition dipole from $|g\rangle$ to $|e\rangle$ is 1.65 ea_0 at this level of theory. Accordingly, we can use a z-polarized ultrashort laser pulse with an electric field $\boldsymbol{\varepsilon}(t') = \varepsilon_0 e^{-\frac{t'^2}{\tau^2}} \sin(\omega t')\hat{\boldsymbol{\epsilon}}_z$ to prepare the initial state $|\Psi(t=0)\rangle = (c_g|g\rangle + c_e|e\rangle)\chi_{g,\mathbf{0}}(\mathbf{Q})$. Here $t' = 0$ is slightly ahead of $t = 0$, such that $|\Psi(t=0)\rangle$ is prepared when the laser field is off. As an example, we choose $c_g = \sqrt{\frac{9}{10}}$ and $c_e = \sqrt{\frac{1}{10}}$ for subsequent calculations. The corresponding laser parameters can be chosen as $E_0 = 3.0 \times 10^9$ V/m and $\hbar\omega = \Delta E_{eg}^{\rm vertical}$, respectively. In this case, the corresponding intensity is below the upper limit, $I_{max} = 2.4 \times 10^{12}$W/cm^2. The pulse duration can be estimated to be $\tau \approx 1$ fs. This enables the approximation of frozen nuclei during the laser pulse. We will not focus on the numerical simulation of initial state preparation since such kind of initial state has already been prepared experimentally for this molecule.[51,52] In addition, the essence of the results reported in this work is robust even if the initial state may have a different and more general form such as $c_g|g\rangle\chi_{g,\mathbf{0}}(\mathbf{Q}) + c_e|e\rangle\chi_e(\mathbf{Q})$, which will be discussed below.

For $t > 0$, the system will propagate freely, leading to the time-dependent electron density $\rho_{\rm el}(\mathbf{r},t)$ in Eq. (31). It can be written as the sum of a time-independent part $\rho_{\rm el,0}(\mathbf{r})$ and a fluctuating part $\Delta\rho_{\rm el}(\mathbf{r},t)$,

$$\begin{aligned} \rho_{\rm el}(\mathbf{r},t) &= \rho_{\rm el,0}(\mathbf{r}) + \Delta\rho_{\rm el}(\mathbf{r},t), \\ \rho_{\rm el,0}(\mathbf{r}) &= |c_g|^2 \rho_{gg}^{(0)}(\mathbf{r}) + |c_e|^2 \rho_{ee}^{(0)}(\mathbf{r}). \end{aligned} \quad (32)$$

Here $\Delta\rho_{\rm el,0}(\mathbf{r})$ consists of the zero-order diagonal terms of $\rho_{\rm el}(\mathbf{r},t)$. Since $\mathbf{Q}_g^{eq} = 0$ the expression of $\Delta\rho_{\rm el}(\mathbf{r},t)$ can be simplified as

$$\begin{aligned} \Delta\rho_{\rm el}(\mathbf{r},t) = |c_e|^2 \sum_j \Delta Q_j \rho_{ee,j}^{(1)}(\mathbf{r})[1 - \cos(\omega_{ej}t)] \\ + 2\,\mathrm{Re}\left\{ C_{ge}(t) S_{ge}(t) \left[\rho_{ge}^{(0)}(\mathbf{r}) + \sum_j \rho_{ge,j}^{(1)} \frac{\langle Q_j(t)\rangle_{ge}}{S_{ge,j}(t)} \right] \right\}, \end{aligned} \quad (33)$$

where

$$\Delta Q_j = Q_{ej}^{eq} - Q_{gj}^{eq} = Q_{ej}^{eq}, \quad (34)$$

is the shift between the minima of the potential $V_e(Q_j)$ and $V_g(Q_j)$ in Eq. (23) for the jth normal mode. Here Re means the real part. The first term of $\Delta\rho_{\rm el}(\mathbf{r},t)$ is a diagonal ("ee") term contributed by

the first order term in the expansion Eq. (28). It depends on the trajectories of the vibrational modes j [cf. the first row of Eq. (25)]. The other terms of $\Delta\rho_{\rm el}(\mathbf{r},t)$ [in the second row of Eq. (33)] are off-diagonal ("eg") contributions of the zero order and first order terms in the expansion of Eq. (28). These off-diagonal contributions are proportional to the overlap $S_{ge}(t)$ of the nuclear wavefunctions in the ground ($|g\rangle$) and excited ($|e\rangle$) states, i.e., they characterize the coherence of charge migration.[32–34] Note that the zero order term in the expansion of Eq. (28) does not depend on the nuclear motions. In contrast, the first order term of Eq. (28) introduces an additional dependence on the nuclear motions beyond the overlap $S_{ge}(t)$. In the present quantum dynamics simulations for pyrene, it turns out that the effect of the zero order term of Eq. (28) exceeds the first order term by an order of magnitude.

B. Charge migration

In this sub-section, we calculate the time evolution of the electron density of the model pyrene after its preparation in the initial "minimal" superposition state $(c_g|g\rangle + c_e|e\rangle)\chi_{g,\mathbf{0}}(\mathbf{Q})$ with coefficients $c_g = \sqrt{\frac{9}{10}}$ and $c_e = \sqrt{\frac{1}{10}}$, as explained in Sec. III A. The goal is to discover signatures of de- and recoherences in charge migration presented by the electron density, confirming the working hypothesis that has been suggested by the experimental spectra in Refs. 51 and 52. As discussed in Sec. I, the validity of the present quantum dynamics simulations is constrained to the initial rather short time domain below ~43 fs. Nevertheless, we shall present results until 100 fs. For times above 43 fs, these should be considered as adiabatic references for more realistic non-adiabatic calculations, beyond the present approximation by the adiabatic Born–Huang expansion.

For reference, it is helpful to consider the symmetry of charge migration for the case when all nuclei are fixed in the ground state geometry $\mathbf{Q}_g^{\rm eq}$. In this case, the fluctuating part of the electron density has B_{1u} symmetry. For symmetry reasons, there cannot be any net charge migrations along the x- or y-axes. Nuclear motions may induce non-zero components of charge migration along x or y, but they will have much smaller amplitudes than those along the z-axis. For this reason, the subsequent application with moving nuclei focuses on the dynamics of the one dimensional reduced electron density $\rho_{\rm el}(z,t)$. The corresponding fluctuating part of the 1D electron density is

$$\Delta\rho_{\rm el}(z,t) = \iint \Delta\rho_{\rm el}(\mathbf{r},t)dxdy. \tag{35}$$

The spatiotemporal propagation of $\Delta\rho_{\rm el}(z,t)$ is shown in Fig. 2(a) for $t < 100$ fs by a color-coded contour plot. Signals of ultrafast charge migration can be identified in many different time windows. They typically have similar patterns but different amplitudes of charge migration. Apparently, the pattern of $\Delta\rho_{\rm el}(z,t)$ confirms the working hypothesis, i.e., the model pyrene exhibits quasi-periodic charge migration with de- and recoherences. The corresponding quasi-period of charge migration is slightly above 1 fs; the times for de- and re-coherences are of the order of 11 fs and 22 fs, respectively.

For better quantitative analysis, we now apply the third method of development, beyond previous representations of electronic charge migration with de- and recoherences.[13,25] For this purpose, we use the corresponding electron flux, or flux density,[49] along the z-axis. It is obtained by the 1D continuity equation[49] as

$$F_z(z,t) = -\int_{-\infty}^{z} \frac{\partial}{\partial t}\Delta\rho_{\rm el}(z',t)dz'. \tag{36}$$

From a physical point of view, the electron flux $F_z(z,t)$ is an observable that directly characterizes the phenomenon of charge migration. Positive and negative values of $F_z(z,t)$ mean charge migration along the positive and negative directions of the z-axis, respectively. The spatiotemporal propagation of $F_z(z,t)$ is illustrated in Fig. 2(b) for $t < 100$ fs. Charge migration can be clearly identified in Fig. 2(b). In addition, there is an apparent decoherence of charge migration in about 11 fs, followed by the first partial recoherence of charge migration at about 22 fs. Decoherences and partial recoherences occur repeatedly, similar to the processes in $HCCI^+$ that have been discovered in Ref. 39. An important property of pyrene is that the amplitude of charge migration never decreases to zero for $t < 100$ fs.

To reveal further details of charge migration in pyrene, we show enlarged plots of $\Delta\rho_{\rm el}(z,t)$ and $F_z(z,t)$ for $t < 20$ fs in Figs. 2(c) and 2(d), respectively. For better inspection of the charge migration, we mark the positions of all the carbon atoms of the pyrene molecule on the top of each panel of Fig. 2 as small black dots. The D_{2h} symmetry of pyrene implies that its 16 carbon atoms have only eight different values of the z-coordinates. For simplicity, the 16 carbon atoms will be grouped as $C_1, C_2, \ldots, C_8$ according to the ascending order of their z coordinates. In Fig. 2(c), the electron density around C_2 first decreases and then increases during about 1 fs. In contrast, the electron density around C_3 first increases and then decreases during the same period. This corresponds to the electron flux $F_z(z,t)$ from C_2 to C_3 and back shown in Fig. 2(d), which is positive for the first half period and negative for the second half period. Similarly, we can identify charge migrations from C_4 to C_5 and from C_6 to C_7. The primary components of charge migration are thus unidirectionally from $C_2/C_4/C_6$ to $C_3/C_5/C_7$ during the first half period and back in the next half period. By careful inspection of Fig. 2, we can further identify charge migration from C_2/C_8 to C_1/C_7 and back in the same period.

Figures 2(a) and 2(c) also reveal a complementary component of charge migration that is much slower than the one discussed earlier. The most obvious signals of the slow component appear close to $z = \pm 2a_0$ [cf. the red pattern from about $t \approx 5$ fs to $t \approx 15$ fs in Fig. 2(c)]. Figure 2(a) shows that close to $z \approx \pm 2a_0$, the slow component of $\Delta\rho_{\rm el}(z,t)$ oscillates quasi-periodically with a period slightly larger than 20 fs. Different from the fast charge migration, the slow signals do not exhibit decoherences. This can be explained by the first term of $\Delta\rho_{\rm el}(\mathbf{r},t)$ in Eq. (33) that is responsible for the slow electron dynamics. We can even recognize its interference with the signal of fast charge migration. This leads to a modulation of the signal for the fast charge migration (with a period just above 1 fs) such that close to 11 fs it is slightly longer than near 0 fs or near 22 fs. As a consequence, at the time close to 22 fs when this signal documents partial recoherence of charge migration, it is phase-shifted with respect to the original signal close to 0 fs. The phase shift is 0.97π. This effect correlates well with the corresponding experimental phase shift by π at the time of partial recoherence.[51,52] The reason for the slow electron dynamics is that some electrons follow the vibrations of the nuclei. The time scale of nuclear vibrations is much

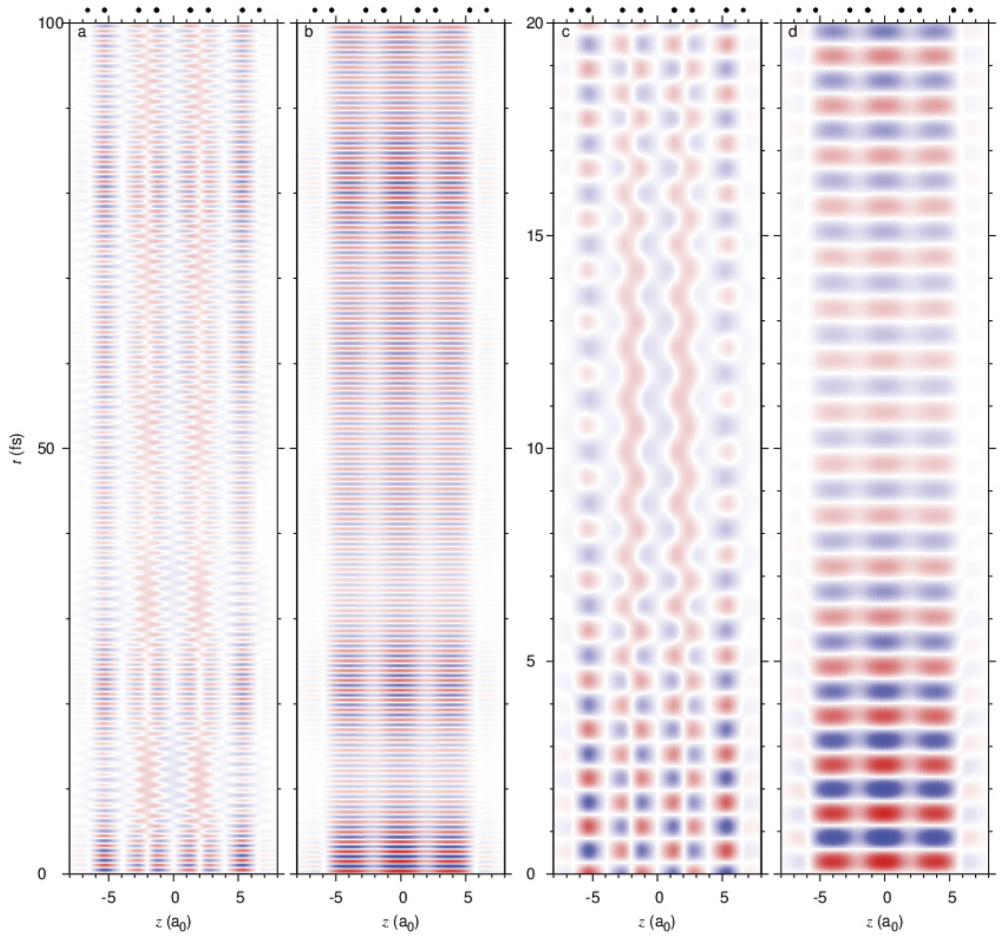

FIG. 2. Electron dynamics and charge migration with de- and recoherences in pyrene along the *z*-axis. (a) The fluctuating part of the electron density $\Delta\rho_{el}(z,t)$ for $t < 100$ fs. (b) The electron flux $F_z(z,t)$ for $t < 100$ fs. (c) Enlarged plot of (a) for $t < 20$ fs. (d) Enlarged plot of (b) for $t < 20$ fs. The color-codings of (a)–(d) are the same. Red and blue colors represent positive and negative contour-values, respectively. In (a)–(d), the maximum/minimum values of $\Delta\rho_{el}(z,t)$ and $F_z(z,t)$ are $\pm 0.1\ a_0^{-1}$ and $\pm 0.8\ \text{fs}^{-1}$, respectively.

longer than that of charge migration. The slow electron dynamics also contributes to the total electron flux $F_z(z,t)$. However, this contribution is about two orders of magnitude smaller than that of the fast charge migration. As a consequence, the flux contributed by the slow electron dynamics in the vicinities of $z \approx \pm 2a_0$ is not visible for the graphical resolution of Figs. 2(b) and 2(d).

C. Effects of nuclear motions: Decoherences and recoherences of charge migration

Figure 2 shows charge migration back and forth in certain regions of the pyrene molecule, as discussed earlier. The amplitudes of the time-dependent parts of the electron density representing charge migration in different regions are different. But they vary concertedly with time. The variations in the amplitudes of charge migration determine the decoherences and recoherences, which are the primary effects of nuclear motions. To investigate the decoherences and recoherences of charge migration quantitatively, we show cuts of the electron flux $F_z(z,t)$ at selected fixed values of z in Figs. 3(b)–3(d). The overlap between the nuclear wavepackets of the electronic states $|g\rangle$ and $|e\rangle$, namely, $S_{ge}(t)$ in Eq. (30), is also investigated. For comparison, $|S_{ge}(t)|$ is shown in Fig. 3(a).

Decoherences and recoherences of charge migration can be characterized by the envelops of Figs. 3(b)–3(d). Specifically, the first decoherence of charge migration in each panel of Figs. 3(b)–3(d) lasts from $t = 0$ to $t \approx 11.6$ fs. However, the coherence of charge migration increases from $t \approx 11.6$ fs to $t \approx t_1^{\text{rev}} = 22.0$ fs. We can further identify new decoherences and partial recoherences in Figs. 3(b)–3(d). As can be seen, the decoherences and partial recoherences of charge migration in Figs. 3(b)–3(d) correlate well with the decays and partial revivals of the nuclear overlap $|S_{ge}(t)|$ in Fig. 3(a), irrespective of the different choices of values of z for

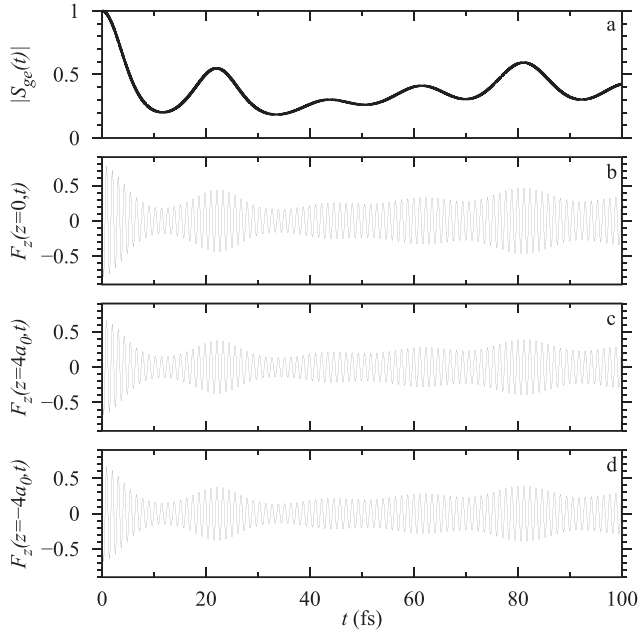

FIG. 3. Quantitative representation of decoherences and recoherences of charge migration in pyrene. (a) The absolute value of the overlap of the two nuclear wavefunctions of the ground and first bright states. (b) Cut of Fig. 2(b) for the electron flux $F_z(z,t)$ at $z = 0$. (c) Same as (b), but for $z = 4a_0$. (d) Same as (b), but for $z = -4a_0$.

$F_z(z,t)$. At $t = 0$, the nuclear overlap in Fig. 3(a) has its maximum value $|S_{ge}(t=0)| = 1$. It decays in about 10 fs, reaching its minimum value $|S_{ge}|_{\min} = 0.2$ at $t = 11.6$ fs. Subsequently, $|S_{ge}(t)|$ increases with time to reach the value of the first partial revival $|S_{ge}(t)| = 0.55$ at $t_1^{\text{rev}} = 22.0$ fs. The next two partial revivals occur at $t_{2,3}^{\text{rev}} = 43.8,\ 61.5$ fs, respectively. Finally, the largest partial revival for the investigated time window in Fig. 3(a) is found at $t_4^{\text{rev}} = 81.1$ fs, with $|S_{ge}(t)| = 0.59$. The time windows $[t_n^{\text{rev}}, t_{n+1}^{\text{rev}}]$ for the decays and partial revivals of the nuclear overlap [Fig. 3(a)] agree well with the time windows for the decoherences and partial recoherences of charge migration [Figs. 3(b)–3(d)], respectively.

Apparently, the decoherences and recoherences are caused by nuclear vibrations. Specifically, they are caused by the vibrations of 72 normal modes of pyrene. In general, the contributions of different modes to the decoherence may differ significantly. For pyrene, the detailed contributions of each normal mode are documented in Table I. For this purpose, the 72 normal modes are classified into two groups. The modes in the first and second groups are documented in the upper and lower parts of Table I, separated by a horizontal line. The modes in the first group have A_g symmetry. Consequently, they have nonzero shifts between the equilibrium structures of the electronic ground and excited states. The component of the shift along the jth normal mode is ΔQ_j in Eq. (34), which is listed in the third column of Table I. The modes in the second group belong to the other irreversible representations of D_{2h} different from A_g. Due to symmetry reasons, they have $\Delta Q_j = 0$, namely, the minima of the ground-state and the excited-state potentials are both exactly located at $Q_j = 0$.

The total overlap between the nuclear wavepackets of the two electronic states $|g\rangle$ and $|e\rangle$ can be factorized as $S_{ge}(t) = \prod_{j=1}^{N} S_{ge,j}(t)$ [cf. Eq. (29)]. The contribution of the jth mode to the decoherence is negligible provided $S_{ge,j}(t) \approx 1$ for all the time. Consequently, we quantitatively characterize the contribution of the jth mode to the decoherence by the value of $1 - |S_{ge,j}(t)|_{\min}$, as listed in the last column of Table I. The analytical expression of $S_{ge,j}(t)$ depends on ΔQ_j and on the frequency shift $\Delta\omega_j \equiv \omega_{ej} - \omega_{gj}$. In the fourth column of Table I, we provide the values of the relative frequency shift $\frac{\Delta\omega_j}{\omega_{gj}}$. Apparently the frequency shifts for the first group of normal modes with A_g symmetry are all negligible. With the approximation $\omega_{ej} \approx \omega_{gj}$, the expression $|S_{ge,j}(t)|$ can be simplified as

$$|S_{ge,j}(t)| \approx \mathrm{e}^{-\omega_{ej}\Delta Q_j^2[1-\cos(\omega_{ej}t)]/2\hbar}. \tag{37}$$

The normal mode frequency ω_{ej} of the electronically excited state and the period of $|S_{ge,j}(t)|$ are provided in the 5th and 6th columns of Table I. For the first part of Table I, the numerical results for Eq. (29) agree well with Eq. (37).

Concerning the second part of Table I (the last four rows), the value of ΔQ_j is exactly zero. In this case, the expression of $|S_{ge,j}(t)|$ can be simplified as

$$|S_{ge,j}(t)| \approx \left[\cos^2(\omega_{ej}t) + \left(\frac{\omega_{gj}^2 + \omega_{ej}^2}{2\omega_{gj}\omega_{ej}}\right)^2 \sin^2(\omega_{ej}t)\right]^{-\frac{1}{4}}. \tag{38}$$

For the last four rows of Table I, the results of the approximation Eq. (38) agree well with the accurate results for Eq. (29). Table I shows that the contributions to the electronic decoherence caused by vibrational frequency shifts are much smaller than the ones caused by nonzero shifts between the two equilibrium structures. The largest relative frequency shift in Table I is almost 20%. However, its contribution to the decoherence is only about $\frac{1}{40}$ of the largest one in the first part of Table I.

Table I reveals that for the model pyrene, there are only a few normal modes that play important roles in the decoherence of charge migration. This is further demonstrated in Fig. 4. Specifically, we put the normal modes in order of their importance for the decoherence and check the convergence of $S_{ge}(t)$ by including the modes one by one (cf. Table I). The simplest model includes modes 62 and 8, namely, the two most important modes, leading to the red dashed curve in Fig. 4. This already imprints the basic structure of $|S_{ge}(t)|$; compare the result for all modes (black solid). A better convergence can be achieved by including the next mode 47 (cf. the green dotted curve). Further including the next mode 52 leads to almost converged results of $S_{ge}(t)$, as documented by the small differences between the blue and black curves in Fig. 4.

Note that the initial state that can be prepared by experiments may be different from our assumption in Sec. III A. For example, the excited-state wavepacket may be different from $\chi_{g,\mathbf{0}}(\mathbf{Q})$ at $t = 0$ if it is prepared by a relatively long laser pulse (e.g., $\tau = 18$ fs in Refs. 51 and 52). Accordingly, the modulus of the initial nuclear overlap $|S_{ge}(t=0)|$ is smaller than 1. In this case, one should still observe the repeated decoherences and recoherences of charge migration, albeit with a smaller initial amplitude compared to the present ideal case with 100% initial electronic coherence.

TABLE I. Contributions of individual normal modes to the decoherence of pyrene prepared in a superposition of the electronic ground state $|g\rangle$ and the first bright excited state $|e\rangle$.

Normal mode j	Symmetry[a]	$\lvert\Delta Q_j\rvert$[b] $(m_e^{\frac{1}{2}} a_0)$	$\lvert\frac{\omega_{ej}-\omega_{gj}}{\omega_{gj}}\rvert$[c]	ω_{ej} (c cm^{-1})	$T(\lvert S_{ge,j}\rvert)$[d] (fs)	Decoherence[e]
8	A_g	17.21	0.0047	411.0	81.2	0.4271
62	A_g	8.96	0.0343	1641.2	20.3	0.4620
47	A_g	8.27	0.0165	1259.0	26.5	0.3292
52	A_g	7.48	0.0113	1440.8	23.1	0.3101
17	A_g	4.63	0.0018	605.1	55.1	0.0574
41	A_g	4.36	0.0203	1143.0	29.2	0.0962
37	A_g	1.40	0.0044	1094.9	30.5	0.0097
24	A_g	0.87	0.0032	814.0	41.0	0.0028
58	A_g	0.37	0.0408	1551.0	21.5	0.0011
70	A_g	0.19	0.0010	3202.6	10.4	0.0005
72	A_g	0.17	0.0007	3210.8	10.4	0.0004
65	A_g	0.13	0.0012	3186.8	10.5	0.0002
4	B_{1g}	0	0.1944	201.9	82.6	0.0115
56	B_{2u}	0	0.1485	1312.7	12.7	0.0064
13	B_{2g}	0	0.1213	456.0	36.6	0.0042
Others	⋯	0	≤0.0939	⋯	⋯	≤0.0024

[a]The table is divided by the horizontal line into the upper and lower parts for normal modes with irreducible representations A_g and others (B_{1g}, etc.), respectively. Modes j = 8, 62, 47, and 52 causing strong decoherence are illustrated in Fig. 1.
[b]Shift of the potential minima in Eq. (34).
[c]Relative frequency shift [cf. Eqs. (19)–(23)].
[d]Period of the overlap $S_{ge,j}(t)$ of the nuclear wavefunctions of the mode j in states $|g\rangle$ and $|e\rangle$.
[e]The decoherence is quantified as $1 - |S_{ge,j}(t)|_{\min}$ (see text).

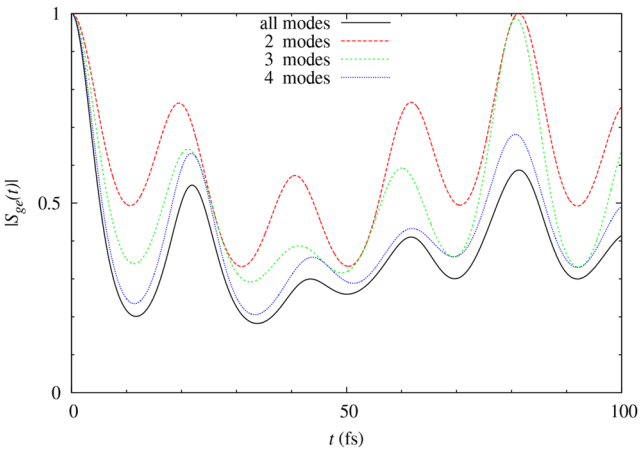

FIG. 4. Convergence of the nuclear overlap $S_{ge}(t)$ of pyrene, cf. Fig. 3(a). The black solid curve is the numerical result of $S_{ge}(t)$ including all 72 normal modes of pyrene. The red, green, or blue results are the numerical result of $S_{ge}(t)$ by including only the most important two, three, or four normal modes (labeled j = 8, 62, 47, 52; cf. Table I), respectively.

IV. CONCLUSIONS

We have discovered charge migration with de- and recoherences in the model pyrene ($C_{16}H_{10}$). This result confirms the underlying working hypothesis, which has been motivated by experimental spectra.[51,52] Still, it is surprising in view of the fact that until today, the phenomenon has been documented only for much smaller molecules or molecular ions, specifically in diatomic molecules[28,32] and in small polyatomic molecules or ions, namely, in $HCCI^+$,[39] in the model fulvene with a reduced set of five different totally symmetric modes (out of 24),[41] and in SiH_4.[38] Chemical intuition would not suggest the present result, but rather it would predict that increasing numbers of vibrational modes (72 for the model pyrene!) should suppress recoherences.[33]

The present result for the model pyrene has been analyzed in detail. This allows us to derive some general criteria that should support charge migration with de- and recoherences in polyatomic molecules as large as (or even larger than) pyrene. (a) Prominent decoherences in superpositions of two electronic states of polyatomic molecules can be caused by normal mode vibrations if the minima of the corresponding PES are shifted with respect to each other. (b) For comparison, any frequency shifts are much less important. (c) This motivates the search for polyatomic candidates with very small shifts of the potential minima in the superimposed states. (d) Gratifyingly, normal modes of symmetric molecules have zero shifts of the potential minima if the corresponding irreducible representations (IRREPs) are different from the highest IRREP, where all the characters are equal to one. (e) Hence, suitable polyatomic candidates should be highly symmetric with many different IRREPs such that most normal modes do not have the highest IRREP. We note in passing that, rewardingly, the first experimental observation of charge migration with de- and recoherences has been made in

the highly symmetric (T_d) proof-of-principle, SiH_4.[38] (f) In general, the molecular equilibrium structures in the superimposed electronic states should coincide as much as possible in order to avoid any shifts of the corresponding potential minima along the normal modes for the highest IRREP. (g) It is advantageous to prepare superpositions in only two states because it would be more difficult to realize the criterion (f) if one prepares the polyatomic molecule in a superposition of more than two states.

These criteria explain *a posteriori* why pyrene has served as a successful first example for the experimental discovery of recoherence in a polyatomic molecule:[51,52] It is highly symmetric (D_{2h}), and the shift of the potential minima in the equilibrium structures of pyrene in the ground and the first bright excited states is very small compared to many other molecules.[54]

The results have been obtained by means of quantum dynamics simulations of the time evolution of the coupled electrons and nuclei in a superposition of two electronic states. To this end, we have employed well established methods that have already been successfully applied to literally hundreds of rather small polyatomic molecules, namely, the "minimal" adiabatic Born–Huang expansion of the total molecular wavefunction, with additional approximations, e.g., time-dependent (non-frozen!) Gaussians for the time evolution of the vibrational modes (see, e.g., Ref. 37). The present success rests, however, on two extensions of the method, namely, the direct visualization of the charge migration with de- and recoherences in terms of the time dependent electron density and flux instead of the previous indirect documentation in terms of the overlap of nuclear wavefunctions. The high resolutions of the temporal and spatial fluctuations of the electron density and flux even allowed the quantum dynamical simulation of the experimental π-shift of the phase of the recoherence; this effect could never be resolved in terms of the time evolution of the overlap of the rather slowly moving nuclear wavefunctions. In addition, we also developed an approximate theory for quantum dynamics simulation of the preparation of the initial superposition of electronic states by means of an ultrashort laser pulse. Unfortunately, however, we were unable to simulate the experimental preparation of the same initial state by means of two rather long (~15 fs) laser pulses, because this causes rather complex interferences of the electric field of the laser and the quasi-periodic charge migration.

The present approach should be considered a rather simple reference. Clearly, it calls for extensions such as the simulation of the preparation of the initial superposition state by much longer laser pulses, the incorporation of nonadiabatic couplings, or nuclear motions in anharmonic potentials. This way, it may serve as a step toward the discovery of large polyatomic molecules that maintain long-lasting coherences or provide efficient recoherences in electronic superposition states for various potential applications such as quantum computations, quantum information, and quantum engineering. Understanding de- and recoherence effects of laser-induced charge migration in polyatomic molecules should also contribute to one of the most important challenges of attosecond chemistry, namely, quoting the stimulating perspective by Merrit *et al.*,[64] to "trigger the desired electron dynamics, allowing for control of consequent nuclear motion"…"which was first inspired by the initial experiments[2]" on charge migration in oligopeptides (see also the literature on recent progress in laser control of electrons quoted in Ref. 64, together with Refs. 40 and 65). Merritt *et al.*[64] conclude that "a large amount of theoretical and experimental work remains to be performed, however, before 'true' atto-chemistry—charge-directed reactivity achieved by direct control of electrons in a system—can be realized."

ACKNOWLEDGMENTS

One of us (J.M.) expresses sincere thanks to Professor E. Riedle and to his wife, Professor R. de Vivie-Riedle (L. M. Universität München), for in-depth discussions of the experiment that discovered recoherences in pyrene (cf. Refs. 51 and 52). We are also grateful to Professor D. Sundholm (The University of Helsinki) for providing the results of Ref. 53 prior to publication, and to Professor J. C. Tremblay (Université Lorraine) for guidance and advice to the modular python toolbox ORBKIT[66–68] for the calculation of the electron density. This work profits from financial support provided in part by the National Key Research and Development Program of China (Grant No. 2017YFA0304203), the Program for Changjiang Scholars and Innovative Research Team (Grant No. IRT_17R70), the National Natural Science Foundation of China (Grant No. 11904215), the 111 Project (Grant No. D18001), the Fund for Shanxi 1331 Project Key Subjects Construction, and the Hundred Talent Program of Shanxi Province.

AUTHOR DECLARATIONS

Conflict of Interest

The authors have no conflicts to disclose.

Author Contributions

HuiMin Ma: Data curation (equal); Formal analysis (equal). **Jörn Manz**: Conceptualization (equal); Writing – original draft (equal); Writing – review & editing (equal). **HuiHui Wang**: Data curation (equal); Funding acquisition (equal); Validation (equal); Writing – review & editing (equal). **YiJing Yan**: Conceptualization (equal); Methodology (equal); Writing – original draft (equal); Writing – review & editing (equal). **Yonggang Yang**: Funding acquisition (equal); Methodology (equal); Supervision (equal); Writing – original draft (equal); Writing – review & editing (equal).

DATA AVAILABILITY

The data that support the findings of this study are available within the article.

REFERENCES

[1] H. Eyring, J. Walter, and G. E. Kimball, *Quantum Chemistry* (Wiley, New York, 1994), Chap. 11.

[2] R. Weinkauf, P. Schanen, D. Yang, S. Soukara, and E. W. Schlag, "Elementary processes in peptides: Electron mobility and dissociation in peptide cations in the gas phase," J. Phys. Chem. **99**, 11255 (1995).

[3] F. Remacle, R. D. Levine, E. W. Schlag, and R. Weinkauf, "Electronic control of site selective reactivity: A model combining charge migration and dissociation," J. Phys. Chem. A **103**, 10149 (1999).

[4] L. S. Cederbaum and J. Zobeley, "Ultrafast charge migration by electron correlation," Chem. Phys. Lett. **307**, 205 (1999).

[5]S. Chelkowski, G. L. Yudin, and A. D. Bandrauk, "Observing electron motion in molecules," J. Phys. B **39**, S409 (2006).
[6]F. Remacle, M. Nest, and R. D. Levine, "Laser steered ultrafast quantum dynamics of electrons in LiH," Phys. Rev. Lett. **99**, 183902 (2007).
[7]M. Nest, F. Remacle, and R. D. Levine, "Pump and probe ultrafast electron dynamics in LiH: A computational study," New J. Phys. **10**, 025019 (2008).
[8]M. F. Kling, P. von den Hoff, I. Znakovskaya, and R. de Vivie-Riedle, "(sub-) femtosecond control of molecular reactions via tailoring the electric field of light," Phys. Chem. Chem. Phys. **15**, 9448 (2013).
[9]P. M. Kraus, B. Mignolet, D. Baykusheva, A. Rupenyan, L. Horný, E. F. Penka, G. Grassi, O. I. Tolstikhin, J. Schneider, F. Jensen, L. B. Madsen, A. D. Bandrauk, F. Remacle, and H. J. Wörner, "Measurement and laser control of attosecond charge migration in ionized iodoacetylene," Science **350**, 790 (2015).
[10]H. J. Wörner, C. A. Arrell, N. Banerji, A. Cannizzo, M. Chergui, A. K. Das, P. Hamm, U. Keller, P. M. Kraus, E. Liberatore, P. Lopez-Tarifa, M. Lucchini, M. Meuwly, C. Milne, J.-E. Moser, U. Rothlisberger, G. Smolentsev, J. Teuscher, J. A. van Bokhoven, and O. Wenger, "Charge migration and charge transfer in molecular systems," Struct. Dyn. **4**, 061508 (2017).
[11]G. Hermann, V. Pohl, G. Dixit, and J. C. Tremblay, "Probing electronic fluxes via time-resolved X-ray scattering," Phys. Rev. Lett. **124**, 013002 (2020).
[12]A. S. Folorunso, A. Bruner, F. Mauger, K. A. Hamer, S. Hernandez, R. R. Jones, L. F. DiMauro, M. B. Gaarde, K. J. Schafer, and K. Lopata, "Molecular modes of attosecond charge migration," Phys. Rev. Lett. **126**, 133002 (2021).
[13]A. Ferté and M. Vacher, "Recent advances in theoretical attosecond chemistry," Chem. Modell. **17**, 153 (2022).
[14]I. Barth and J. Manz, "Periodic electron circulation induced by circularly polarized laser pulses: Quantum model simulations for Mg porphyrin," Angew. Chem., Int. Ed. **45**, 2962 (2006).
[15]I. Barth, J. Manz, Y. Shigeta, and K. Yagi, "Unidirectional electronic ring current driven by a few cycle circularly polarized laser pulse: Quantum model simulations for Mg-Porphyrin," J. Am. Chem. Soc. **128**, 7043 (2006).
[16]M. Kanno, H. Kono, and Y. Fujimura, "Control of pi-electron rotation in chiral aromatic molecules by nonhelical laser pulses," Angew. Chem., Int. Ed. **45**, 7995 (2006).
[17]I. S. Ulusoy and M. Nest, "Correlated electron dynamics: How aromaticity can be controlled," J. Am. Chem. Soc. **133**, 20230 (2011).
[18]M. Yamaki, H. Mineo, Y. Teranishi, M. Hayashi, Y. Fujimura, H. Nakamura, and S. H. Lin, "Quantum localization of coherent π-electron angular momentum in (P)-2,2'-biphenol," J. Phys. Chem. Lett. **5**, 2044 (2014).
[19]K.-J. Yuan, C.-C. Shu, D. Dong, and A. D. Bandrauk, "Attosecond dynamics of molecular electronic ring currents," J. Phys. Chem. Lett. **8**, 2229 (2017).
[20]C. Liu, J. Manz, K. Ohmori, C. Sommer, N. Takei, J. C. Tremblay, and Y. Zhang, "Attosecond control of restoration of electronic structure symmetry," Phys. Rev. Lett. **121**, 173201 (2018).
[21]C. Liu, J. Manz, H. Wang, and Y. Yang, "Quantum engineering of helical charge migration in HCCI," Chin. Phys. Lett. **39**, 123402 (2022).
[22]D. Jia, J. Manz, B. Paulus, V. Pohl, J. C. Tremblay, and Y. Yang, "Quantum control of electronic fluxes during adiabatic attosecond charge migration in degenerate superposition states of benzene," Chem. Phys. **482**, 146 (2017).
[23]K. Takatsuka, "Electron dynamics in molecular elementary processes and chemical reactions," Bull. Chem. Soc. Jpn. **94**, 1421 (2021).
[24]D. Jia, J. Manz, A. Schild, V. Svoboda, and Y. Yang, "From nuclear fluxes during tunnelling to electronic fluxes during charge migration," in *Tunnelling in Molecules: Nuclear Quantum Effects from Bio to Physical Chemistry* (Royal Society of Chemistry, 2020), Chap. 5.
[25]Y. Shu and D. G. Truhlar, "Decoherence and its role in electronically nonadiabatic dynamics," J. Chem. Theory Comput. **19**, 380 (2023).
[26]D. J. Diestler, G. Hermann, and J. Manz, "Charge migration in Eyring, Walter and Kimball's 1944 model of the electronically excited hydrogen-molecule ion," J. Phys. Chem. A **121**, 5332 (2017).
[27]A. D. Bandrauk, S. Chelkowski, P. B. Corkum, J. Manz, and G. L. Yudin, "Attosecond photoionization of a coherent superposition of bound and dissociative molecular states: Effect of nuclear motion," J. Phys. B **42**, 134001 (2009).
[28]P. von den Hoff, R. Siemering, M. Kowalewski, and R. de Vivie-Riedle, "Electron dynamics and its control in molecules: From diatomics to larger molecular systems," J. Select. Top. Quantum Electron. **18**, 119 (2012).
[29]V. Despré, A. Marciniak, V. Loriot, M. C. E. Galbraith, A. Rouzée, M. J. J. Vrakking, F. Lépine, and A. I. Kuleff, "Attosecond hole migration in Benzene molecules surviving nuclear motion," J. Phys. Chem. Lett. **6**, 426 (2015).
[30]Z. Li, O. Vendrell, and R. Santra, "Ultrafast charge transfer of a valence double hole in glycine driven exclusively by nuclear motion," Phys. Rev. Lett. **115**, 143002 (2015).
[31]M. Vacher, L. Steinberg, A. J. Jenkins, M. J. Bearpark, and M. Robb, "Electron dynamics following photoionization: Decoherence due to nuclear-wave-packet width," Phys. Rev. A **92**, 040502(R) (2015).
[32]A. Nikodem, R. D. Levine, and F. Remacle, "Quantum nuclear dynamics pumped and probed by ultrafast polarization controlled steering of a coherent electronic state in LiH," J. Phys. Chem. A **120**, 3343 (2016).
[33]C. Arnold, O. Vendrell, and R. Santra, "Electronic decoherence following photoionization: Full quantum-dynamical treatment of the influence of nuclear motion," Phys. Rev. A **95**, 033425 (2017).
[34]M. Vacher, M. J. Bearpark, M. Robb, and J. P. Malhado, "Electron dynamics upon ionization of polyatomic molecules: Coupling to quantum nuclear motion and decoherence," Phys. Rev. Lett. **118**, 083001 (2017).
[35]V. Despré, N. V. Golubev, and A. I. Kuleff, "Charge migration in propiolic acid: A full quantum dynamical study," Phys. Rev. Lett. **121**, 203002 (2018).
[36]N. V. Golubev, T. Begušić, and J. Vaníček, "On-the-fly *ab initio* semiclassical evaluation of electronic coherences in polyatomic molecules reveals a simple mechanism of decoherence," Phys. Rev. Lett. **125**, 083001 (2020).
[37]A. Scheidegger, J. Vaníček, and N. V. Golubev, "Search for long-lasting electronic coherence using on-the-fly *ab initio* semiclassical dynamics," J. Chem. Phys. **156**, 034104 (2022).
[38]D. T. Matselyukh, V. Despré, N. V. Golubev, A. I. Kuleff, and H. J. Wörner, "Decoherence and revival in attosecond charge migration driven by non-adiabatic dynamics," Nat. Phys. **18**, 1206 (2022).
[39]D. Jia, J. Manz, and Y. Yang, "De- and recoherence of charge migration in ionized iodoacetylene," J. Phys. Chem. Lett. **10**, 4273 (2019).
[40]D. Jia, J. Manz, and Y. Yang, "Timing the recoherences of attosecond electronic charge migration by quantum control of femtosecond nuclear dynamics: A case study for $HCCI^+$," J. Chem. Phys. **151**, 244306 (2019).
[41]A. Csehi, P. Badankó, G. J. Halász, Á. Vibók, and B. Lasorne, "On the preservation of coherence in the electronic wavepacket of a neutral and rigid polyatomic molecule," J. Phys. B **53**, 184005 (2020).
[42]D. Jia, J. Manz, and Y. Yang, "Generation of electronic flux during the femtosecond laser pulse tailored to induce adiabatic attosecond charge migration in $HCCI^+$," J. Mod. Opt. **64**, 960 (2017).
[43]M. Born and K. Huang, *Dynamical Theory of Crystal Lattices* (Oxford University Press, 1954).
[44]M. Born and R. Oppenheimer, "Zur Quantentheorie der Molekeln," Ann. Phys. **84**, 457 (1927).
[45]D. J. Diestler, "Beyond the Born–Oppenheimer approximation: A treatment of electronic flux density in electronically adiabatic molecular processes," J. Phys. Chem. A **117**, 4698 (2013).
[46]D. J. Diestler, J. Manz, and J. F. Pérez-Torres, "Comparison of approximate methods for computation of the concerted adiabatic electronic and nuclear fluxes in aligned H_2^+ ($^2\Sigma_g^+$)," Chem. Phys. **514**, 66 (2018).
[47]M. F. Flórez-Angarita and J. F. Pérez-Torres, "Photoionization of oriented $HD(^1\Sigma^+)$ yields vibrating $HD^+(^2\Sigma^+)$ with charge breathing and small charge transfer," J. Phys. Chem. A **126**, 8918 (2022).
[48]D. Mendive-Tapia, M. Vacher, M. J. Bearpark, and M. A. Robb, "Coupled electron-nuclear dynamics: Charge migration and charge transfer initiated near a conical intersection," J. Chem. Phys. **139**, 044110 (2013).
[49]T. Bredtmann, D. J. Diestler, S.-D. Li, J. Manz, J. F. Pérez-Torres, W.-J. Tian, Y.-B. Wu, Y. Yang, and H.-J. Zhai, "Quantum theory of concerted electronic and nuclear fluxes associated with adiabatic intramolecular processes," Phys. Chem. Chem. Phys. **17**, 29421 (2015).

[50]J. R. Platt, "Classification of spectra of cata-condensed hydrocarbons," J. Chem. Phys. **17**, 484 (1949).
[51]N. Krebs, I. Pugliesi, J. Hauer, and E. Riedle, "Two-dimensional Fourier transform spectroscopy in the ultraviolet with sub-20 fs pump pulses and 250-720 nm supercontinuum probe," New J. Phys. **15**, 085016 (2013).
[52]N. Krebs, "New insights for femtosecond spectroscopy," PhD thesis, Ludwig-Maximilians-Universität München, 2013, see https://edoc.ub.uni-muenchen.de/21902/.
[53]I. Benkyi, E. Tapavicza, H. Fliegl, and D. Sundholm, "Calculation of vibrationally resolved absorption spectra of acenes and pyrene," Phys. Chem. Chem. Phys. **21**, 21094 (2019).
[54]M. K. Roos, S. Reiter, and R. de Vivie-Riedle, "Ultrafast relaxation from ^1L_a to ^1L_b in pyrene: A theoretical study," Chem. Phys. **515**, 586 (2018).
[55]J. Ferguson, L. W. Reeves, and W. G. Schneider, "Vapor absorption spectra and oscillator strengths of naphthalene, anthracene, and pyrene," Can. J. Chem. **35**, 1117 (1957).
[56]J. B. Briks, *Photophysics of Aromatic Molecules* (Wiley, New York, 1970).
[57]Y.-L. Wang and G.-S. Wu, "Improving the TDDFT calculation of low-lying excited states for polycyclic aromatic hydrocarbons using the Tamm-Dancoff approximation," Int. J. Quantum Chem. **108**, 430 (2008).
[58]E. J. Heller, "Time-dependent approach to semiclassical dynamics," J. Chem. Phys. **62**, 1544 (1975).
[59]D. J. Tannor, *Introduction to Quantum Mechanics: A Time-dependent Perspective* (University Science Books, Sausalito, CA, 2006).
[60]G. W. Richings, I. Polyak, K. E. Spinlove, G. A. Worth, I. Burghardt, and B. Lasorne, "Quantum dynamics simulations using Gaussian wavepackets: The vMCG method," Int. Rev. Phys. Chem. **34**, 269 (2015).
[61]B. Crawford, Jr, "Vibrational intensities. II. the use of isotopes," J. Chem. Phys. **20**, 977 (1952).
[62]M. J. Frisch, G. W. Trucks, H. B. Schlegel *et al.*, GAUSSIAN 09, Revision B.01, Gaussian Inc., Wallingford, CT, 2010.
[63]H. J. Werner, P. J. Knowles, G. Knizia *et al.*, MOLPRO, version 2012.1, a package of *ab initio* programs, 2012, see http://www.molpro.net.
[64]I. C. D. Merritt, D. Jacquemin, and M. Vacher, "Attochemistry: Is controlling electrons the future of photochemistry?." J. Phys. Chem. Lett. **12**, 8404 (2021).
[65]D. Dey, A. I. Kuleff, and G. A. Worth, "Quantum interference paves the way for long-lived electronic coherences," Phys. Rev. Lett. **129**, 173203 (2022).
[66]G. Hermann, V. Pohl, J. C. Tremblay, B. Paulus, H.-C. Hege, and A. Schild, "Orbkit: A modular python toolbox for cross-platform postprocessing of quantum chemical wavefunction data," J. Comput. Chem. **37**, 1511 (2016).
[67]G. Hermann, V. Pohl, and J. C. Tremblay, "An open-source framework for analyzing n-electron dynamics. II. Hybrid density functional theory/configuration interaction methodology," J. Comput. Chem. **38**, 2378 (2017).
[68]V. Pohl, G. Hermann, and J. C. Tremblay, "An open-source framework for analyzing n-electron dynamics. I. Multideterminantal wave functions," Chem. Phys. **38**, 1515 (2017).